International Journal for Housing Science and Its Applications
Publish August 4, 2025. Volume 46, Issue 3 Pages 2848-2862

https://doi.org/10.70517/ijhsa463239

Dynamic analysis of quantum entanglement and quantum state transport mechanisms based on electromagnetic wave action

Hao Zhang[1,*]
[1] Weinan Normal University, Weinan, Shaanxi, 714099, China
Corresponding authors: (e-mail: zhanghao1726@126.com).

Abstract Based on the relevant concepts of quantum entanglement and the basic principles of quantum information, this paper focuses on the generation process of three-body high-dimensional entangled states between magnets and photons in the Uptime (PT)-symmetry-breaking phase, and clarifies the dissipation and evolution process of three-body high-dimensional entangled states for the system in this paper. Finally, it is generalized to the hybrid photon-magneton oscillator system in the action of electromagnetic waves to explore whether the perfect transmission of quantum states can be realized under the condition of one-dimensional magnetic oscillator open-chain arrangement. The results show that the introduction of three-body high-dimensionality can not only effectively enhance the entanglement, but also effectively enhance the entanglement resistance to environmental interference, so that the system can operate stably in a wider range of parameters. The scheme in this paper can utilize the optical cavity dissipation to keep the quantum state stable at the receiving end. In addition, the spontaneous radiation of atoms is significantly suppressed due to the adiabatic elimination of the excited state, which makes the scheme more robust. Meanwhile, based on the existing experimental techniques, the scheme has high experimental feasibility, and the fidelity of its transmitted state at the receiving end can reach more than 99.74%.

Index Terms Quantum entanglement, Electromagnetic wave action, Hybrid photon-magnetic oscillator system, Quantum state transmission mechanism

I. Introduction

The use of quantum systems such as coherent manipulation to achieve a variety of information processing is quantum information processing, which includes many aspects, such as quantum computing, quantum stealth transmission and quantum key distribution [1]-[3]. The advantages of quantum information processing compared with the traditional information processing, on the one hand, in computing speed and information capacity, on the other hand, in providing a strong guarantee for information security, and the problems that cannot be solved by classical computers, quantum computers may be able to solve [4]-[7]. Quantum state transfer (QST) has been a hot research topic in the field of quantum information processing, which requires that arbitrary quantum states can be coherently transferred from the “transmitting” system to the “receiving” system [8]. The entangled state is a special property of matter in the microscopic world, and the mechanical nature of the relationship between subsystems and degrees of freedom in a quantum system can also be characterized by quantum entangled states [9]. To characterize this peculiar quantum phenomenon, it can be explained in a composite system formed by several subsystems using the principle of superposition of states in quantum mechanics [10], [11]. By realizing quantum state transport and preparing entangled states, thus providing strong technical support for the rapid development of quantum information [12], [13].

Modern physics shows that the macroscopic so-called electromagnetic waves are microscopically composed of a large number of electromagnetic wave quanta, each of which has its own physical quantities such as energy, momentum, angular momentum, etc [14], [15]. By controlling the physical quantities of electromagnetic wave quanta to change according to certain laws at the transmitting end of the communication system, while detecting and recording them at the receiving end, the information desired to be transmitted can be known and the purpose of wireless communication can be realized [16]-[18]. Therefore, analyzing the quantum entanglement and quantum state transmission mechanism under the action of electromagnetic waves can further develop wireless communication, improve the transmission rate and spectral efficiency, and provide a completely new dimension for the transmission system [19], [20].

In this paper, we first introduce quantum entanglement and quantum mechanics, quantum bits, and quantum

operational gates, based on which a hybrid system of a non-Ermian superconducting quantum circuit with YIG, consisting of two microwave cavities and a yttrium iron garnet (YIG) sphere, is studied. The Hamiltonian quantities of the system and its energy spectrum are derived analytically, and abundant singularities, PT-symmetric phases and PT-symmetric broken phases are studied in parameter space. The oscillations appearing in three-body high-dimensional entangled states as well as quantum coherence under the PT-symmetric phase and the steady states generating three-body high-dimensional entangled states as well as quantum coherence under the PT-symmetry-breaking phase are investigated as a means of clarifying the effect of three-body high-dimensional entangled states on the dissipation of the hybrid system. Based on the frequency modulation theory, a tunable magnetic oscillator-magnetic oscillator coupling is obtained by utilizing the dielectric of the coupled cavity. The coupling strength is made to satisfy the perfect transmission condition by modulating the frequency parameters. In order to further verify the correctness of the theoretical analysis, numerical simulations are carried out to prove the feasibility of the model in this paper.

II. Quantum entanglement and quantum state transport mechanism based on electromagnetic wave action

II. A. Quantum Entanglement

II. A. 1) The concept of quantum entangled states

Quantum entanglement [21] is a unique quantum mechanical phenomenon distinct from classical systems, and before introducing the concept of quantum entangled states, the definition of separable states is first given. If the state ρ_{AB} of a quantum system can be expressed as a linear superposition of the direct products of several uncorrelated states, i.e., there are:

$$\rho_{AB} = \sum_i p_i \rho_A^i \otimes \rho_B^i \quad (\sum_i p_i = 1) \tag{1}$$

Then the state of the system is said to be a separable state, which can be pure or mixed. If the state of a quantum system cannot be written in the form of a separable state, then it is called an entangled state. An entangled state can be either a pure state or a mixed state.

Bell state is a typical two-body entangled state, which consists of the following four states:

$$|\varphi^+\rangle_{AB} = \frac{|0\rangle_A |1\rangle_B + |1\rangle_A |0\rangle_B}{\sqrt{2}} \tag{2}$$

$$|\varphi^-\rangle_{AB} = \frac{|0\rangle_A |1\rangle_B - |1\rangle_A |0\rangle_B}{\sqrt{2}} \tag{3}$$

$$|\phi^+\rangle_{AB} = \frac{|0\rangle_A |0\rangle_B + |1\rangle_A |1\rangle_B}{\sqrt{2}} \tag{4}$$

$$|\phi^-\rangle_{AB} = \frac{|0\rangle_A |0\rangle_B - |1\rangle_A |1\rangle_B}{\sqrt{2}} \tag{5}$$

The Bell state is the simplest two-body entangled state, in which the states of both particle A and particle B are indeterminate prior to the measurement; a measurement is made on one of the particles, and the state of the other particle is determined.

II. A. 2) The EPR feint and Bell's inequality

The EPR feint verifies that quantum mechanics is correct, thus supporting Bell's view.Bell's inequality states that if definite-domain positivism holds, an arbitrary system should satisfy the following equation:

$$\left| p(a,b) - p(a,c) \right| \le 1 + p(b,c) \tag{6}$$

where $p(a,b) = \int \rho(\lambda) A(a\lambda) B(b\lambda) d\lambda$, λ is a hidden variable, $\rho(\lambda)$ is its distribution function, $A(a\lambda)$ is the result of Alice's measurements of particle 1's spin along the a direction, and $B(b\lambda)$ is the result of Bob's measurements of particle 2's spin along the b direction. spin, and $B(b\lambda)$ is the result of Bob's measurement of particle 2's spin along the b direction. For particles with spin 1/2, $A(a\lambda) = \pm 1, B(b\lambda) = \pm 1$.

The best known of the many generalized forms of Bell's inequality is the CHSH inequality below:

$$E(QS)+E(RS)+E(RT)-E(QT)\le 2 \tag{7}$$

Q,R is the result obtained by Alice's two random measurements of particle 1, S,T is the result obtained by Bob's two random measurements of particle 2, and the value of Q,R,S,T is either +1 or -1.

II. A. 3) Metrics of quantum entanglement

For different quantum entangled states, the strength of their entanglement is different, so it is necessary to introduce the concept of entanglement degree, so as to quantize the degree of quantum entanglement. The definitions of several commonly used entanglement degrees are introduced below:

(1) Partial entropy entanglement degree

For two-body pure state, its partial entropy entanglement degree is defined as:

$$E_p(|\varphi\rangle_{AB})=S(\rho_A)=S(\rho_B) \tag{8}$$

$S(\rho_A)$ is the von Neumann entropy.

For two-body mixed states, the partial entropy entanglement degree is defined as:

$$E_p=\frac{S(\rho_A)+S(\rho_B)-S(\rho_{AB})}{2} \tag{9}$$

(2) Relative entropy entanglement degree

For a two-body quantum state ρ_{AB}, the relative entropy entanglement degree is defined as:

$$E_r(\rho_{AB})=\min S(\rho_{AB}\|\sigma_{AB}) \tag{10}$$

σ_{AB} is a separable state and $S(\rho_{AB}\|\sigma_{AB})$ is the relative entropy of ρ_{AB} with respect to σ_{AB}:

$$S(\rho_{AB}\|\sigma_{AB})=tr[\rho_{AB}(lb\rho_{AB}-lb\sigma_{AB})] \tag{11}$$

(3) Formation entanglement degree

For a two-body quantum state ρ_{AB}, the formation entanglement degree is defined as follows:

$$E_f(\rho_{AB})=\min\sum_i p_i E_p(|\varphi_i\rangle_{AB}) \tag{12}$$

where $\{p_i,|\varphi_i\rangle_{AB}\}$ is any decomposition of ρ_{AB}, $\rho_{AB}=\sum_i p_i|\varphi_i\rangle_{AB}\langle\varphi_i|$, and $|\varphi_i\rangle_{AB}$ is not required here to be mutually orthogonal, but should be a normalized pure state of both bodies. $E_p(|\varphi_i\rangle_{AB})$ is the partial entanglement entropy of $|\varphi_i\rangle_{AB}$.

(4) The purifiable entanglement degree

If Alice and Bob share N two-body quantum states ρ_{AB}, and the maximum number of EPR pairs obtained by the two through local operation and classical communication is $k(N)$, the purifiable entanglement degree is defined as:

$$D(\rho_{AB})=\lim\frac{k(N)}{N} \tag{13}$$

II. A. 4) Quantum Entanglement Criterion

It is often difficult to determine whether a many-body quantum state is entangled or not. A Schmidt number criterion for determining the pure state of two-body entanglement is introduced below.

Schmidt decomposition theorem: let $|\psi\rangle$ be a pure state of the composite system AB, then there exists a standard orthogonal basis $|n_A\rangle$ of the subsystem A and a standard orthogonal basis $|n_B\rangle$ of the subsystem B such that:

$$|\psi\rangle=\sum_n \lambda_n|n_A\rangle|n_B\rangle \tag{14}$$

The $|n_A\rangle,|n_B\rangle$ is called the Schmidt basis of the subsystem A,B. The λ_n are called Schmidt coefficients, are nonnegative real numbers and satisfy $\sum\lambda_n^2=1$. The number of nonzero λ_n is called the Schmidt number of $|\psi\rangle$.

Schmidt number criterion: for a two-body pure state $|\psi\lambda_{AB}$ consisting of subsystems A and subsystems B, a quantum state is entangled if its Schmidt number > 1.

II. B.Quantum Information Fundamentals

II. B. 1) Quantum bits

(1) Basic quantum bit

A quantum bit [22], abbreviated as qubit, is used to describe a quantum state with many properties that distinguish it from a classical bit.

Defining an arbitrary state vector $|\psi\rangle$ in a two-dimensional Hilbert space as a fundamental quantum bit, with base vectors $|0\rangle$ and $|1\rangle$ in that space, the quantum bit $|\psi\rangle$ can be expressed as:

$$|\psi\rangle=\alpha|0\rangle+\beta|1\rangle \tag{15}$$

α and β are complex numbers satisfying $|\alpha|^2+|\beta|^2=1$. A quantum bit $|\psi\rangle$ can be in the $|0\rangle$ state or the $|1\rangle$ state, or in a superposition of the two, which is the biggest difference from a classical bit.

Hilbert space can have multiple sets of basis vectors, even for the same quantum bit, if different basis vectors are chosen, there are different manifestations. To wit:

$$|+\rangle=\frac{1}{\sqrt{2}}(|0\rangle+|1\rangle),|-\rangle=\frac{1}{\sqrt{2}}(|0\rangle-|1\rangle) \tag{16}$$

A quantum bit can be represented as:

$$|\psi\rangle=\frac{\sqrt{2}}{2}(\alpha+\beta)|+\rangle+\frac{\sqrt{2}}{2}(\alpha-\beta)|-\rangle \tag{17}$$

The $|0\rangle,|1\rangle$ basis is usually referred to as the computational basis vector and the $|+\rangle,|-\rangle$ basis as the physical basis vector.

A fundamental quantum bit can be represented in the following form:

$$|\psi\rangle=e^{i\gamma}(\cos(\frac{\theta}{2})|0\rangle+e^{i\varphi}\sin(\frac{\theta}{2})|1\rangle) \tag{18}$$

The angular parameters γ,φ,θ form a spherical coordinate system. The $e^{i\gamma}$ is a phase factor and does not have any observable effect on the quantum state, thus the above equation can be rewritten as:

$$|\psi\rangle=\cos(\frac{\theta}{2})|0\rangle+e^{i\varphi}\sin(\frac{\theta}{2})|1\rangle \tag{19}$$

(2) Composite Quantum Bits

θ denotes the angle of this point with the Z-axis, and φ denotes the angle of the projection of this point in the XY-plane with the X-axis. A composite quantum bit refers specifically to a quantum bit consisting of n single-base composite, corresponding to a Hilbert space of dimension n and the number of eigenvectors 2^n, expressed as follows:

$$|\psi\rangle=\alpha_1|0_1 0_2...0_n\rangle+\alpha_2|1_1 0_2...0_n\rangle+...+\alpha_m|1_1 1_2...0_n\rangle+...+\alpha_{2^n}|1_1 1_2...1_n\rangle \tag{20}$$

The subscripts $1,2,...n$ correspond to different single bases respectively, physically representing different particles.

(3) Multi-Binary Quantum Bits

A basic binary quantum bit can be represented by a linear combination of two orthogonal bases, while a multicast quantum bit can be represented by a linear combination of d orthogonal basis vectors:

$$|\psi\rangle=\sum_{k=0}^{d}\alpha_k|k\rangle \tag{21}$$

where d denotes the number of progressions. The space in which a d-variant quantum bit resides is a 2^d-dimensional Hilbert space.

A quantum bit can be a composite multicomponent quantum bit, e.g. a double-base triple-component quantum bit can be represented in the following form:

$$\begin{aligned}|\psi_2^3\rangle = \alpha_{00}|00\rangle + \alpha_{01}|01\rangle + \alpha_{02}|02\rangle + \alpha_{10}|10\rangle \\ +\alpha_{11}|11\rangle + \alpha_{12}|12\rangle + \alpha_{20}|20\rangle + \alpha_{21}|21\rangle + \alpha_{22}|22\rangle\end{aligned} \tag{22}$$

II. B. 2) Properties of quantum bits

The main properties of quantum bits are as follows:

(1) Imprecise measurability.

(2) Non-clonability.

(3) Indistinguishability. If the angle between two quantum bits $|\varphi\rangle,|\phi\rangle$ is θ and $0<\theta<\pi/2$, then the two quantum bits are indistinguishable, and no measurements or manipulations can yield precise results. Define the indistinguishability as:

$$D = |\langle\varphi|\phi\rangle|^2 = cos\theta \tag{23}$$

If two quantum bits are orthogonal, then $D=0$, at which point they are completely distinguishable.

II. B. 3) Quantum Operator Gates

Quantum operational gates are logical operations defined on quantum bits, referred to as quantum gates, which can be represented by an operator matrix. Several typical quantum gates are described below.

(1) Single-bit quantum gate

a) Non-gate (Bubbleley X-gate)

The function of the non-gate operation is to interchange the $|0\rangle,|1\rangle$ positions in a single quantum bit, i.e.:

$$X = \begin{bmatrix}0 & 1\\ 1 & 0\end{bmatrix} \tag{24}$$

Writing the quantum bits $\alpha|0\rangle+\beta|1\rangle$ in vector form $[\alpha\ \beta]^T$, the output of the X gate is:

$$X\begin{bmatrix}\alpha\\ \beta\end{bmatrix} = \begin{bmatrix}\beta\\ \alpha\end{bmatrix} \tag{25}$$

b) Bubble Y Gate

The effect of the Bubbleley Y gate is to change $|0\rangle$ into $i|1\rangle$ and $|1\rangle$ into $-i|0\rangle$. The operator matrix is:

$$Y = \begin{bmatrix}0 & -i\\ i & 0\end{bmatrix} \tag{26}$$

c) The Pauli Z-gate

The Pauli Z-gate produces no change to $|0\rangle$ and changes $|1\rangle$ to $-|1\rangle$ with an operator matrix of:

$$Z = \begin{bmatrix}1 & 0\\ 0 & -1\end{bmatrix} \tag{27}$$

d) Hadhmagate

The Hadema gate changes $|0\rangle$ into $|+\rangle$ and $|1\rangle$ into $|-\rangle$ with the operator matrix:

$$H = \frac{1}{\sqrt{2}}\begin{bmatrix}1 & 1\\ 1 & -1\end{bmatrix} \tag{28}$$

e) Phase Gate

The phase gate turns $\alpha|0\rangle+\beta|1\rangle$ into $\alpha|0\rangle+i\beta|1\rangle$ with an operator matrix of:

$$S = \begin{bmatrix}1 & 0\\ 0 & i\end{bmatrix} \tag{29}$$

(2) Multi-bit quantum gates

a) Controlled non-(CNOT) gate

A controlled nongate is a typical two-bit quantum gate. The two input quantum bits are a control bit and a target bit, and the target bit remains unchanged if the control bit is $|0\rangle$, and the target bit is flipped if the control bit is $|1\rangle$. The operator matrix of a CNOT gate is:

$$U_{CN}=\begin{bmatrix}1&0&0&0\\0&1&0&0\\0&0&0&1\\0&0&1&0\end{bmatrix} \tag{30}$$

b) Swap gate

A swap gate is also a two-bit quantum gate that serves to swap the values of two input quantum bits, corresponding to the operator matrix:

$$U_{SW}=\begin{bmatrix}1&0&0&0\\0&0&1&0\\0&1&0&0\\0&0&0&1\end{bmatrix} \tag{31}$$

II. C. Generation of three-body high-dimensional magneton-photon entangled states

II. C. 1) Generation of three-body two-dimensional entangled states

This section focuses on the process of generating three-body two-dimensional entangled states between magnets and photons in the Uptime [23] (PT)-symmetry breaking phase. First, the evolution process of the hybrid system can be modeled by the master equation:

$$\frac{\partial\rho}{\partial t}=-i[\mathrm{H}_1,\rho]-i\{\mathrm{H}_2,\rho\}+2i\langle\mathrm{H}_2\rangle\rho \tag{32}$$

where $\mathrm{H}_1(\mathrm{H}_2)$ is the Hermitian operator that rerepresents the effective Hamiltonian as $\mathrm{H}_1\equiv(H+H^{\dagger})/2(\mathrm{H}_2\equiv(H-H^{\dagger})/2)$, and $\langle\mathrm{H}_2\rangle=tr(\rho\mathrm{H}_2)$, with parentheses $[\cdot]$ and $\{\cdot\}$ representing the right and against operators, respectively. By adding a third term to keep $tr(\rho)=1$. By solving the evolution equation (32) with respect to the density operator ρ, the initial state $|\phi_0\rangle=|001\rangle_{a,b,c}$ is chosen to be pure and the average particle number state of the initial state is $N=\langle a^{\dagger}a+b^{\dagger}b+c^{\dagger}c\rangle=1$. Then, non-local patterns are introduced:

$$A_{1,2}=\frac{a\pm be^{-i\theta}}{\sqrt{2}} \tag{33}$$

Assume $\omega_a=\omega_b=\omega$ and the large detuning condition $|\omega-\omega_c-r|\square|g|$. Converted to a plotted view of the interaction in a non-local mode, the Hamiltonian quantity can be expressed as:

$$H_{eff}=g_{eff}(A_1^{\dagger}c+A_1c^{\dagger}e^{i\phi}) \tag{34}$$

where $A_1=(a+be^{-i\theta})/\sqrt{2}$ and $g_{eff}=g/\sqrt{2}$. Accordingly, the hybrid system evolves in a finite subspace $\{|\tilde{0}1\rangle_{A_1,c},|\tilde{1}0\rangle_{A_1,c}\}$, where $|\tilde{0}\rangle_{A_1}$ and $|\tilde{1}\rangle_{A_1}$ are the Fock states of the pattern A_1, which evolve within the basis vectors $\{|0\rangle_a,|1\rangle_a,|0\rangle_b,|1\rangle_b\}$ is denoted as $|00\rangle_{a,b}$ and $(|10\rangle_{a,b}+e^{i\theta}|01\rangle_{a,b})/\sqrt{2}$ under . By solving the eigenequation $H|\phi_m\rangle=\omega_m|\phi_m\rangle$, the eigenstates of the hybrid system can be expressed as:

$$|\phi_m\rangle=\cos\theta_m|\tilde{1}0\rangle_{A_1,c}+e^{i\psi_m}\sin\theta_m|\tilde{0}1\rangle_{A_1,c} \tag{35}$$

where θ_m as well as ψ_m are related to the equation $e^{i}\psi_m\tan\theta_m=(\omega_k-\omega)/g(k=1,2,3...)$ correlation. If the initial state is set to be $\rho_0=|\tilde{0}1\rangle_{A_1,c}\langle\tilde{0}1|$, the density matrix of the contained time can be further written as:

$$\rho = \frac{\sum_{k,j} p_{k,j} e^{-i\omega_{kj}t} |\phi_k\rangle\langle\phi_j|}{\sum_{k,j} p_{k,j} e^{-i\omega_{kj}t} tr(|\phi_k\rangle\langle\phi_j|)} \tag{36}$$

where $\omega_{k,j} = \omega_k - \omega_j^*$ and $p_{k,j}$ are the coefficients of the expansion. When $t \to \infty$, the density matrix of the steady state is expressed as $\rho(\infty) = |\phi_1\rangle\langle\phi_1|$. On the one hand, the steady state can be expressed as $|\phi_1\rangle = (|\tilde{1}0\rangle_{A_1,c} + i|\tilde{0}1\rangle_{A_1,c})/\sqrt{2}$, which is the general form of the Bell state under the basis vector $\{|\tilde{0}1\rangle_{A_1,c}, |\tilde{1}0\rangle_{A_1,c}\}$. On the other hand, under the basis vectors $\langle|0\rangle_a, |1\rangle_a, |0\rangle_b, |1\rangle_b, |0\rangle_c, |1\rangle_c\}$, is the three-body entangled state $|\phi_1\rangle = |100\rangle_{a,b,c}/2 + e^{i\theta}|010\rangle_{a,b,c}/2 + i|001\rangle_{a,b,c}/\sqrt{2}$. The parameters $\omega_c/2\pi = 6GHz$, $\omega_a/2\pi = \omega_b/2\pi = 5.95GHz$, $g/2\pi = 6MHz$, and $r/2\pi = 50MHz$, which are experimentally justified under the condition that large detuning is satisfied. The fidelity is defined as $F(t) = tr\sqrt{\langle\phi_1|\rho(t)|\phi_1\rangle}$, where $|\phi_1\rangle$ and $\rho(t)$ are the target states and the time-containing density matrix obtained by solving Equation (32). It is clear that the evolution of the layouts of $|010\rangle_{a,b,c}$ as well as of $|100\rangle_{a,b,c}$ is identical and reaches 0.25 at the last moments of the evolution, whereas the layout of the primitive state $|001\rangle_{a,b,c}$ reaches 0.5 at the last moments. Finally, the layout of the target state $|\phi_1\rangle$ evolves from 0.7 to 1, which indicates that steady-state three-body two-dimensional entangled states can be generated under the $PT-$ symmetry breaking phase.

In a three-body system, quantum coherence may exist due to the collective participation of several subsystems or can be attributed to the coherence within the subsystems. Thus, magneton-photon entanglement can be quantized by collective coherence, which can be expressed as:

$$C = \sqrt{S(\frac{\rho + \rho_\pi}{2}) - \frac{S(\rho) + S(\rho_\pi)}{2}} \tag{37}$$

where s is the von Neumann entropy, ρ is the density matrix of the hybrid system, and the direct product state is denoted as $\rho_\pi \equiv \rho_{min} = \rho_a \otimes \rho_b \otimes \rho_c$. Under the $PT-$ symmetry-breaking phase, the values of F and C are close to 1 and 0.903, respectively, when the dissipation-free system evolves into the ideal three-body entangled state $|\phi_1\rangle$. However, the overall coherence and fidelity of the system are not stabilized under the $PT-$ symmetry phase. Thus, stable three-body entangled states and collective coherence can exist in the $PT-$ symmetry-breaking phase but oscillate in the $PT-$ symmetry phase.

This anomaly can be further understood through the competition between the evolution of non-Ermian systems and the conservation of particle number in hybrid systems. When the hybrid system is in the $PT-$symmetry breaking phase, the evolution of the system guarantees not only gain and loss processes but also particle conservation processes. The coexistence of the two processes evolves the initial state towards the steady state target entangled state. For the $PT-$-symmetric phase, the evolution in the hybrid system exists only in the normalized one, and this evolution is particle number-conserving with beam splitter-type interactions, thus leading to the evolution of the initial state towards the unstable target entangled state.

II. C. 2) Generation of three-body high-dimensional entangled states

When the hybrid system is considered to be under $PT-$ symmetry breaking phase, the hybrid system evolves in $N > 1$ Hilbert subspace. The initial state $|\psi_2\rangle = |\tilde{0}2\rangle_{A1,c}$ is chosen to have an average particle number of $N = 2$. By solving the master equation, a stable three-body three-dimensional entangled state is produced, denoted as:

$$|\phi_2\rangle = \frac{1}{2}|\tilde{2}0\rangle_{A_1,c} - \frac{i}{\sqrt{2}}|\tilde{1}1\rangle_{A_1,c} - \frac{1}{2}|\tilde{0}2\rangle_{A_1,c} \tag{38}$$

where $|\tilde{2}\rangle_{A_1}$ can be expressed under the basis vectors $\{|0\rangle_a, |1\rangle_a, |2\rangle_a, |0\rangle_b, |1\rangle_b, |2\rangle_b\}$ is denoted as $(|20\rangle_a, b + e^{i\theta}\sqrt{2}|11\rangle_{a,b} + e^{2i\theta}|02\rangle_{a,b})/2$. Numerical simulation of the layout evolution of the target state $|\phi_2\rangle$, the initial state $|\psi_2\rangle$, and other evolving states. The general trends are the same for $|101\rangle_{a,b,c}$ and $|011\rangle_{a,b,c}$ ($|020\rangle_{a,b,c}$ and $|200\rangle_{a,b,c}$). The layout of the initial state $|002\rangle_{a,b,c}$ evolves from 1 to 0.25, and the layout of the final

moment $|110\rangle_{a,b,c}$ is close to 0.16. The layout of the target three-body three-dimensional entangled state $|\phi_2\rangle$ is close to 1, and it remains stable at the end of the evolution. This indicates the successful generation of the high-dimensional entangled state of the three-body.

The four-dimensional entangled state of the three-body can be obtained when the average number of particles of the initial state $N=3$ is set and the initial state is chosen as $|\psi_3\rangle=|\tilde{0}3\rangle_{A1,c}$:

$$|\phi_3\rangle=\frac{\sqrt{2}}{4}(\sqrt{3}\,|\tilde{1}2\rangle_{A_1,c}-i\sqrt{3}\,|\tilde{2}1\rangle_{A_1,c}-|\tilde{3}0\rangle_{A_1,c}+i\,|\tilde{0}3\rangle_{A_1,c}) \tag{39}$$

where $|\tilde{3}\rangle_{A_1}$ can be used under the basis vectors $\{|0\rangle_a,|1\rangle_a,|2\rangle_a,|3\rangle_a,|0\rangle_b,|1\rangle_b,|2\rangle_b,|3\rangle_b\}$ is denoted as $(e^{2i\theta}\sqrt{6}\,|12\rangle_{a,b}+e^{i\theta}\sqrt{6}\,|21\rangle_{a,b}+\sqrt{2}\,|30\rangle_{a,b}+e^{3i\theta}\sqrt{2}\,|03\rangle_{a,b})/4$. The fidelity of $|\phi_3\rangle$ in the initial, target, and other evolutionary states reaches 1 and remains stable at the end of the evolution. In the $PT-$ symmetry-breaking phase without considering dissipation, the fidelity of both $|\phi_2\rangle$ and $|\phi_3\rangle$ reaches 1. The final collective coherence of $|\phi_2\rangle$ is 0.917 and 0.944, respectively, and remains stable. The three-body entangled states have larger collective coherence when the half-averaged particle number of the initial state is larger.

In the $PT-$symmetry-breaking phase, the collective coherence maintains a maximum value and stays at a stable value, independent of the size of the detuning. At the same time, the fidelity under $\Delta\approx\pm2.5$ is 1. In the $PT-$ symmetry-breaking phase, the collective coherence and fidelity are oscillatory and do not reach a maximum value. Therefore, the EPs at $\Delta=\pm1.9$ and ±3.1 are the determinants of whether the target three-body high-dimensional entanglement can be produced stably.

II. D.Quantum State Transport

II. D. 1) Perfect transmission of quantum information

Quantum theory was developed in response to the failure of classical physics to account for observed phenomena such as black-body radiation, low-temperature specific heats and cathode-ray diffraction patterns. It extends from atoms and molecules to bulk matter and even to objects on the cosmic scale. A quantum bit is an arbitrary superposition of two classical bits $|0\rangle$ and $|1\rangle$ that can carry information. Two orthogonal states of a quantum system, e.g., two specific energy levels of an atom, the polarization state of a photon, the spin state of an electron, etc., are being used as quantum bits for implementing quantum information protocols.

We give a further introduction to the perfect transmission of quantum information by taking the example of the transmission of photons in a cavity array.

Consider a system N linearly coupled cavities, then the Hamiltonian of the system is $(\hbar=1)$:

$$H=\sum_{l=1}^{N}\omega_l a_l^{\dagger}\hat{a}_l+\sum_{l=1}^{N-1}J_l(a_l^{\dagger}\hat{a}_{l+1}+\hat{a}_l\hat{a}_{l+1}^{\dagger}) \tag{40}$$

where a_l and $a_l^{\dagger}$ are the generation and annihilation operators, respectively, and ω_l is the resonance frequency of the l th cavity. The coupling strength between the l th and $l+1$ th cavities is J_l.

And the perfect transmission of photons requires the correct combination of coupling strengths in the array, i.e:

$$J_l=\sqrt{l(N-l)}J \tag{41}$$

where J is a constant and N is the number of cavities in the array. If the cavities are resonant, the eigenvectors of the Hamiltonian quantity in the single-photon subspace are:

$$|X^{n+1}\rangle=\frac{1}{\sqrt{2^{N-1}}}\sum_{k=0}^{N-1-n}\sum_{k=0}^{n}(-1)^{k'N-1-n}C_kC_{k'}\sqrt{\frac{N-1C_n}{N-1C_r}}\,|r+1\rangle\rangle \tag{42}$$

with eigenvalues $E_{n+1}=(N-1)\omega+(N-1-2n)J$, where $r=n+k-k'$ and $N=0,1,...,N-1$. Here, the state $|r+1\rangle$ denotes the state with a single photon in the $r+1$ th cavity while the other cavities are in the vacuum state. Now, consider a single photon in the first cavity and other cavities in the vacuum state as the initial state, then the initial state is $|1\rangle\rangle=|1\rangle|0\rangle...|0\rangle$, then the state at moment t is:

$$e^{-i\hat{H}t}\,|1\rangle\rangle = e^{-i\hat{H}t}\,|1\rangle|0\rangle...|0\rangle$$
$$= e^{-i\omega t}\sum_{k=0}^{N-1}\sqrt{\binom{N-1}{k}}(\cos Jt)^{N-1-k}(-i\sin Jt)^{k}\,|k+1\rangle\rangle \tag{43}$$

The probability of finding a photon at the end of the array, i.e., in the N th cavity, is:

$$P = |\langle\langle N|e^{-i\hat{H}t}|1\rangle\rangle|^2 = (\sin^2 Jt)^{N-1} \tag{44}$$

Note that the probability P becomes 1 at $t=\pi/2J$, which corresponds to a perfect transfer of photons from the first to the last cavity. Thus, the relationship between the coupling strengths allows for the perfect transfer of photons through the cavity array. This is because position-dependent coupling makes the dispersion relation linear compared to uniform coupling, leading to dispersion-free transmission.

II. D. 2) Derivation of effective Hamiltonian quantities

We proceed to consider the application of the Floquet drive to a hybrid photon-magneto-vibrator system [24], where N yttrium iron garnet (YIG) spheres are arranged according to a one-dimensional open chain and a microwave cavity-magneto-vibrator coupling is established. Using a periodic modulation of the magnetic vibrator mode frequency, the Hamiltonian quantity can be written in the following form:

$$H^{(b)}(t) = H_G^{(b)} + H_A^{(b)}(t) + H_{LM}^{(b)} \tag{45}$$

Among them:

$$\hat{H}_G^{(b)} = \sum_r \omega_0 a_r^{\dagger}\hat{a}_r \tag{46}$$

$$H_A^{(b)}(t) = \sum_i \omega_i(t)\hat{m}_i^{\dagger}\hat{m}_i \tag{47}$$

$$H_{LM}^{(b)} = \sum_{ri} g_{ri}(\hat{m}_i^{\dagger}\hat{a}_r + \hat{m}_i\hat{a}_r^{\dagger}) \tag{48}$$

ω_0 is the cavity frequency, and here we assume that the individual cavity fields have the same frequency. The modulation of the magnetic oscillator mode frequency takes the form $\omega_i(t) = \omega_q + \eta\cos(\omega t)$. $q^{\dagger}$ and $\hat{q}$ ($m_i^{\dagger}$ and m_i) are the production and annihilation operators for cavity photon (magnetic modulus) modes. The g_{ri} denotes the coupling strength between the magnetic oscillator and the microwave cavity.

In order to study the dynamics induced by the magnetic oscillator-magneto-vibrator interaction, we adiabatically annihilate the cavity-photon modes using the SW transform in the large detuned region as follows:

$$U_{sw} = \exp\left\{\sum_{ri} a_{ri}g_{ri}(\hat{m}_i^{\dagger}\hat{a}_r + \hat{m}_i\hat{a}_r^{\dagger})\right\} \tag{49}$$

where $\alpha_{ri} = 1/(\omega_q - \omega_0)$. When the condition g_{ri} □ $\omega_q - \omega_0$ is satisfied, the Hamiltonian quantity can be truncated to second order in the new framework in the following form:

$$H_{sw} = \sum_i \omega_0 a_r^{\dagger}\hat{a} + \sum_{rki} g_{ri}g_{ki}\alpha_{ki}\hat{a}_k^{\dagger}\hat{a} + \hat{a}a^{\dagger}$$
$$+\sum_i \omega_i(t)\hat{m}_i^{\dagger}\hat{m}_i + \sum_{rij} g_{ri}g_{rj}\alpha_{rj}\hat{m}^{\dagger}\hat{m}_i + \hat{m}_j\hat{m}_i^{\dagger} \tag{50}$$

For convenience, let $g_{ri}g_{rj}\alpha_{rj} = g^{(b)}$ and set the cavity field to the vacuum state.

Then, the Hamiltonian quantity is transformed to by the non-interacting part:

$$U_0^{(b)}(t) = e^{-i}\sum_i(\omega_q t + \frac{\eta_i}{\omega}\sin\omega)m_i^{\dagger}\hat{m}_i \tag{51}$$

defined in the interaction plotted view as follows:

$$\hat{H}_I^{(b)}(t) = g^{(b)} \sum_{ij} e^{i\frac{\eta_{ii}}{\omega}\sin\omega t} \hat{m}_i \hat{m}_j^{\dagger} + H.c. \tag{52}$$

where $\eta_{ji} = \eta_j - \eta_i$.

When satisfying ω□ $g^{(b)}$, the Hamiltonian quantity can be rewritten using the Jacobi-Anger expansion preserving to order zero:

$$\hat{H}_I^{(b)} = \sum_{ij} g^{(b)} \mathrm{J}_0(\frac{\eta_{ji}}{\omega}) \hat{m}_i \hat{m}_j^{\dagger} + H.c. \tag{53}$$

where $J_{ij} = g^{(b)} \mathrm{J}_0(\eta_{ji}/\omega)$ is the effective coupling strength, and by modulating the amplitude η, the conditions required for perfect transmission of the quantum state $J_{ij} = \sqrt{i(N-i)}J$.

III. Analysis of dynamical results of quantum entanglement and quantum state transport mechanisms

III. A. Analysis of enhancement results of optical-microwave entanglement and optical-magnetic entanglement

The variation of E_{ac} and E_{am} with the three-body high-dimensional parameters r and θ is shown in Fig. 1, where $\theta = \pi$ and $r = 0.99$. It can be seen that when the reflectivity of the controllable beam splitter is increased from 50% (r=0.71) to 98% (r=0.99), both E_{ac} and E_{am} can be significantly enhanced due to the increasing utilization of the output optical field. In addition, E_{ac} and E_{am} are also very sensitive to the change of phase, and both can reach the entanglement maximum at $\theta = \pi$. After adding the three-body high-dimensional loop, the trends of E_{ac} and E_{am} with the reflection coefficient r and phase θ are basically the same because the entanglement comes from the same source, which is from the entanglement between the optical mode and the phonon, and considering the experimentally feasible conditions, choosing $r = 0.9997, \theta = \pi$, we can obtain optimal three-body high-dimensional enhancement effect on entanglement. In order to compare more comprehensively the optical-microwave entanglement E_{ac} and the optical-magnetic entanglement E_{am} before and after the addition of the three-body high-dimensionality, we need to analyze the relationship between their changes with different parameters.

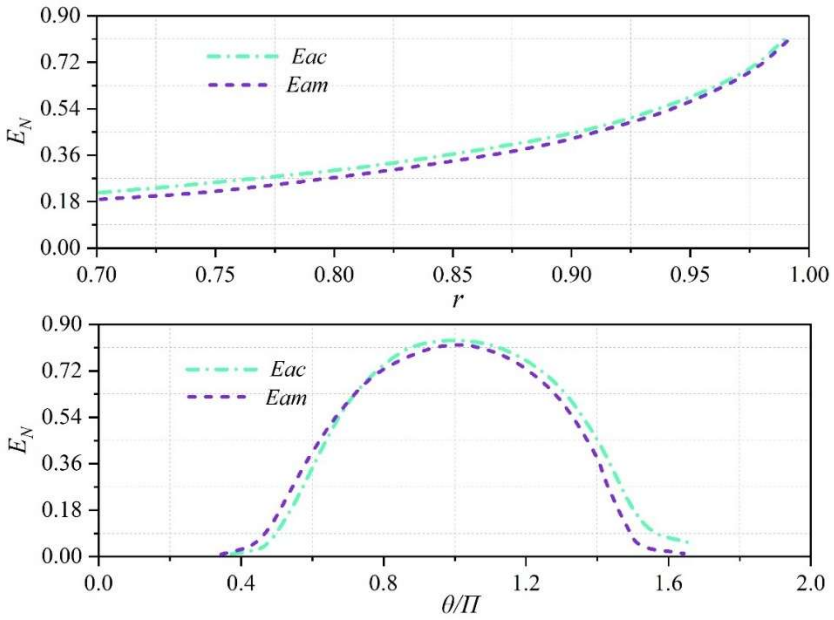

Figure 1: *Eac* and *Eam* versus the coherent feedback parameters *r* and *θ*

The variation of E_{ac} and E_{am} with G_{ab}, G_{cb}, and g_{cm} is shown in Fig. 2, in which (a)~(c) represent G_{ab},

G_{cb}, and g_{cm}, respectively. It can be seen that with the increase of the optical force coupling strength G_{ab}, E_{ac} and E_{am} in the unadded feedback show a tendency to increase and then decrease, which is due to the fact that the generated optical force entanglement E_{ab} gradually increases, and the transfer of E_{ac} and E_{am} to The entanglement also increases, but when G_{ab} increases to a certain level, the phonon mode b mainly interacts with the optical mode a, and the interaction with the microwave mode c is weakened, which leads to a decrease in the entanglement transfer. From Fig. 2(b), it can be seen that with the increase of the microwave-mechanical oscillator coupling strength G_{cb}, E_{ac} and E_{am} in the unaddressed feedback also show a tendency to increase and then decrease, which is due to the fact that the increase of the entanglement transfer capacity makes the transfer to E_{ac} and E_{am} The entanglement of E_{ac} and E_{am} increases, but it increases to a certain extent, the phonon mode b mainly interacts with the microwave mode c, and the interaction with the optical mode a is weakened, which leads to the decrease of the generated entanglement. From Fig. 2(c), it can be seen that as the microwave-magnon coupling strength g_{cm} increases, E_{ac} gradually decreases without feedback, and E_{am} first increases and then decreases due to the gradual transfer of E_{ac} to E_{am}. Obviously, both E_{ac} and E_{am} are substantially boosted by adding three-body higher dimensions, only that different coupling strengths correspond to different magnitudes of the provided lift.

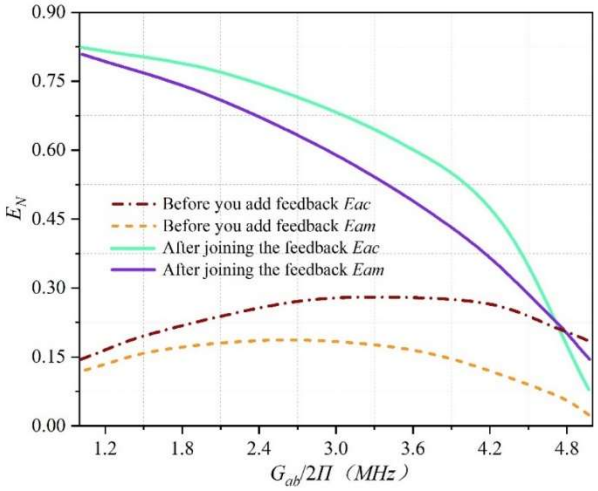

(a)G_{ab}

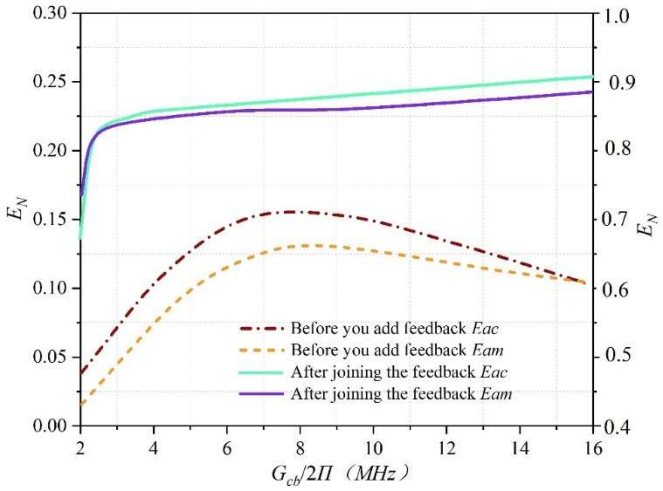

(b)G_{cb}

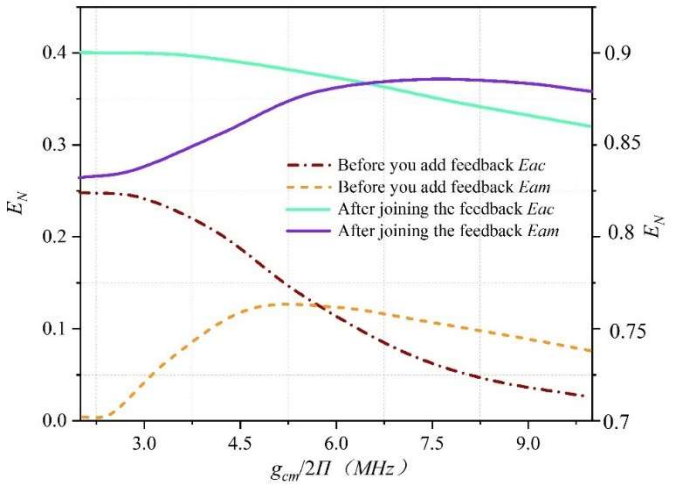

(c)g_{cm}

Figure 2: E_{ac} and E_{am} are related to the change in G_{ab} & G_{cb} & g_{cm}

The variation of E_{ac} and E_{am} with ω_a, ω_c, ω_m is illustrated in Fig. 3, where (a) ~ (c) represent the variation

of ω_a, ω_c and ω_m. It can be seen that ω_a and E_{ac} and E_{am} briefly increase and then gradually decrease with the increase of ω_a without feedback, which is because when ω_a is small, the dissipative coupling is in favor of entanglement generation, only that the magnetic oscillator decay rate (ω_m) is larger, the dissipation-induced decoherence will dominate, which leads to entanglement reduction; however, after adding feedback, with the increase of ω_a, E_{ac} and E_{am} etc. not only significantly enhance but also efficiently maintain this entanglement enhancement, this is because considering the feedback after the equivalent optical mode The effect of the attenuation rate on the entanglement is changed. From Fig. 3(b), it can be seen that both E_{ac} and E_{am} before and after adding the feedback gradually decrease with the increase of ω and the trend of the change is the same, and there is also a significant enhancement of the entanglement after adding the feedback. From Fig. 3(c), it can be seen that as the role played by the increase of ω_m on the entanglement transfer of E_{ac} and E_{am} changes from positive to negative, E_{am} without feedback increases briefly and then decreases gradually, and E_{ac} decreases slightly and then increases gradually after the addition of Feedback, the entanglement is significantly enhanced and changes in the same trend.

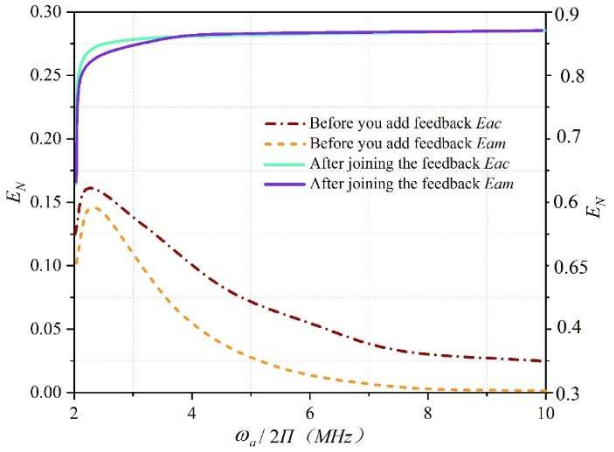

(a) ω_a

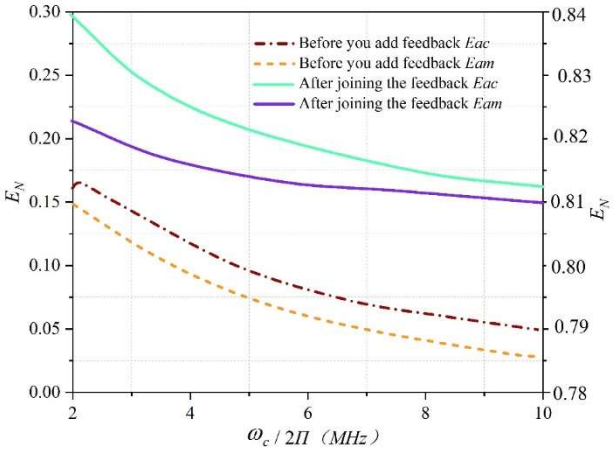

(b) ω_c

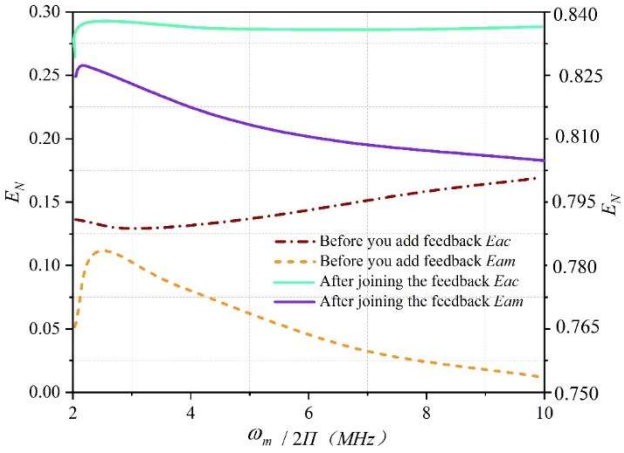

(c) ω_m

Figure 3: E_{ac} and E_{am} are related to the change in ω_a & ω_c & ω_m

The variation of E_{ac} and E_{am} with γ_b and $T_{(b)}$ is shown in Fig. 4, where (a)~(b) represent γ_b and $T_{(b)}$, respectively. It can be seen that the introduction of three-body high-dimensional not only makes the entanglement significantly enhanced but also can be immune to the decay rate of the mechanical oscillator and the change of the temperature to a large extent, especially the optical-magnetic entanglement E_{am} can be well maintained below 12.16 K. This indicates that the introduction of three-body high-dimensional not only effectively enhances the entanglement but

also effectively improves the entanglement's ability of resisting the environmental interference, which makes the system be able to operate stably in a wider range of parameters. It should be noted that all the results in this paper are obtained when the system is in stability, which is guaranteed by the negative real part of the eigenvalues of the coefficient matrix $A_k\,(k=1,2)$.

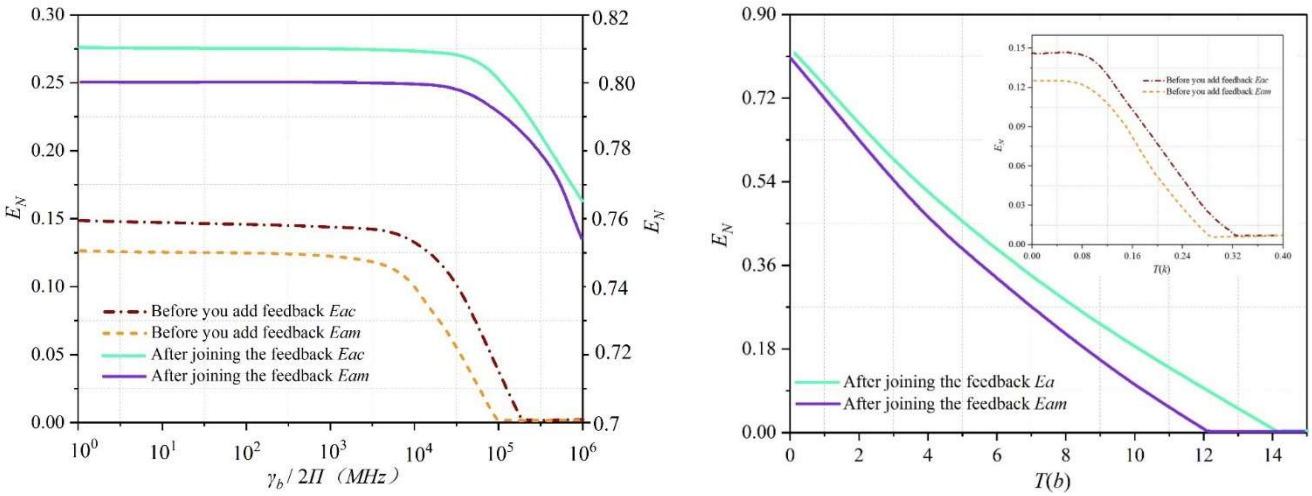

(a)γ_b (b)$T_{(b)}$

Figure 4: E_{ac} and E_{am} are related to the change in γ_b & $T_{(b)}$

III. B. Numerical simulation results of quantum state transport and quantum entanglement

The results of the dynamical evolution of the fidelity of atom 2 in state $|\psi\rangle$ are shown in Fig. 5. The fidelity $F=Tr\left[\left[\rho_s^{1/2}Tr_{1\&c}(\rho)\rho_s^{1/2}\right]^{1/2}\right]$, where $\rho_s=|\psi\rangle\langle\psi|$, and $Tr_{1\&c}$ denotes traces taken for 1-atom and all cavity modes. The parameters of the transport state $|\psi\rangle$ are chosen randomly as $\alpha=\sin\theta,\beta=\cos\theta,\theta=\pi/3$. The ρ_s and pentagrams denote the dynamical evolution of the fidelity F controlled by the original master equation and the effective master equation (H_I replaced by $H_{eff}=H_s^{eff}+H_d^{eff}$), respectively. The overlap of these two curve trajectories fully demonstrates the effectiveness of the simplified system and helps to predict and explain the behavior of the original system. In addition, the fidelity of the state $|\psi\rangle$ is as high as 98.97% at $gt=12000$, and the fidelity of the initial state $|\psi\rangle_1|e\rangle_2|0\rangle_c$ (ρ_o) tends to be close to zero as time nudging tends to zero. These results also confirm the feasibility of our scheme. They show that we can realize the unidirectional transfer of arbitrary quantum states from the “transmitter” system to the “receiver” system and stabilize them in the “receiver” system under time-independent control.

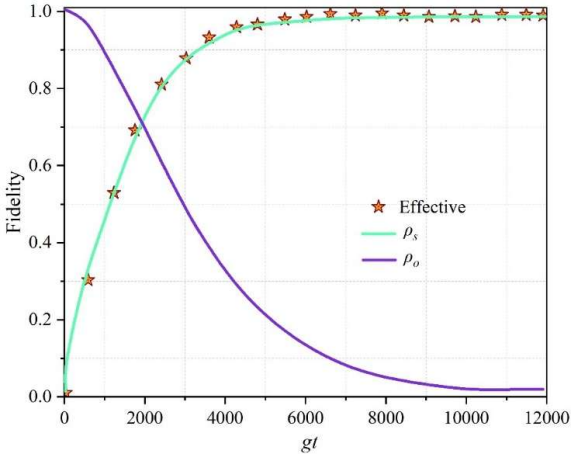

Figure 5: The dynamic evolution of the fidelity of the atom 2 in state $|\psi\rangle$

(Fidelity as a function of gt is governed by the original and effective master equations, where $\rho_s = |\psi\rangle\langle\psi|, \alpha = \sin\theta, \beta = \cos\theta, \theta = \pi/3$. The initial state is $\rho_0 = |\psi\rangle_1\langle\psi| \otimes |e\rangle_1\langle e| \otimes |0\rangle_c\langle 0|$. Other corresponding parameters are: $J = 160g, \delta = 161g, \Omega = 0.01g, \omega = g, \kappa = 0.01g$).

Finally, we analyze the experimental feasibility of the scheme. The applicability and the expected limits of the toroidal microcavity to strongly coupled cavity quantum electrodynamics, where the coupling coefficients can be as high as $g/2\pi = 750$ MHz, are discussed. Based on the corresponding critical photon number and critical atom number, the cavity attenuation rate and atomic spontaneous emissivity for $(\kappa, \gamma)/2\pi = (20.5, 2.5)$ MHz can be obtained. Alternatively, we can assume that two niobium superconducting mirrors ($g/2\pi = 40$ kHz, $k/2\pi = 0.8$ kHz) capture a rubidium atom that has a spontaneous emissivity of $\gamma/2\pi = 0.01$ kHz. And another set of experimental parameters $(g, \kappa, \gamma) = 2\pi \times (140, 5.35, 0.01)$ kHz was obtained.

The dynamic evolution of the experimental parameters on the fidelity of the transport state $|\psi\rangle$ in atom 2 is shown in Fig. 6. Using the above sets of parameters, we calculated the evolution of the fidelity of atom 2 in the state $|\psi\rangle$ with time, and the fidelity is stable at more than 99.74%, and these results fully demonstrate the experimental feasibility of our scheme. In addition, the effect of different values of θ on the fidelity of the transmission state $|\psi\rangle$ is depicted in the inset. The trend of these curves is completely consistent, which faithfully reflects that our scheme is realizable with arbitrary quantum states.

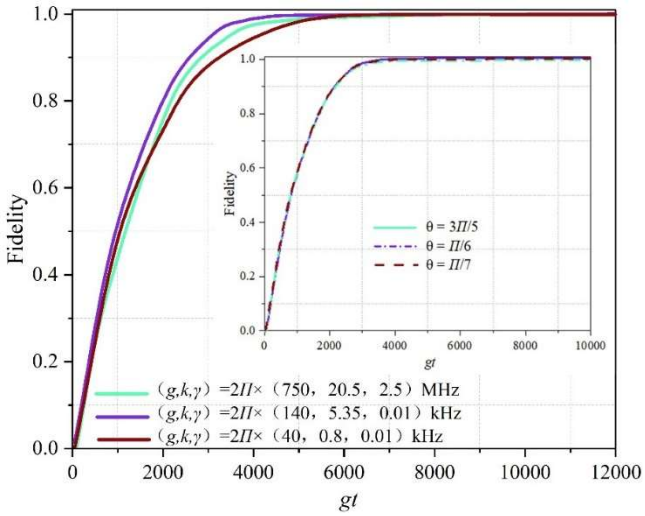

Figure 6: The dynamic evolution of the fidelity of the transmission state $|\psi\rangle$ in atom 2

(Other corresponding parameters are: $J = 160g, \delta = 161g, \Omega = 0.01g, \omega = g, \theta = \pi/3$.) The inset shows the variation in fidelity of the transmitted state $|\psi\rangle$ for different values of θ with the parameters: $g = 2\pi \times 750$ MHz, $\kappa = 20.5$ MHz, $\gamma = 2.5$ MHz, $J = 160$ g, $\delta = 161$ g, $\Omega = 0.01$ g, $\omega = g$.)

IV. Conclusion

In this paper, a scheme to enhance optical-microwave entanglement and photomagnetic entanglement by using three-body high-dimensional photomagnetic system is proposed, the physical mechanisms and conditions of entanglement generation and entanglement transfer are analyzed in detail, the parameter conditions for entanglement optimization are obtained, and on this basis, the change relations of quantum state transport of optical-microwave entanglement and photomagnetic entanglement before and after the addition of three-body high dimensions are compared in detail with those of optical-microwave entanglement and photomagnetic entanglement under different parameters.

(1) After adding three-body high-dimensional, both optical-microwave entanglement and optical-magnetic entanglement can be enhanced more substantially in a wider parameter range, and this enhancement effect can be well maintained.

(2) Due to the dissipation of the optical cavity, arbitrary quantum states can not only be transferred from the "transmitting" system to the "receiving" system, but also can be stabilized in the "receiving" system without external time control. In addition, the excited states of the atoms suppress the spontaneous radiation of the atoms under

appropriate conditions. And the fidelity of the transmission state of the receiving system can reach more than 99.74% under suitable experimental parameters.

The results not only provide strong theoretical support for the realization of hybrid quantum networks, but also offer more possibilities for optical control, design, detection and transmission of magnetic vibrator states, facilitating the ability to manipulate and utilize the quantum properties of magnetic vibrators more flexibly in the future.

References

[1] Blais, A., Girvin, S. M., & Oliver, W. D. (2020). Quantum information processing and quantum optics with circuit quantum electrodynamics. Nature Physics, 16(3), 247-256.

[2] Hu, X. M., Guo, Y., Liu, B. H., Li, C. F., & Guo, G. C. (2023). Progress in quantum teleportation. Nature Reviews Physics, 5(6), 339-353.

[3] Diamanti, E., Lo, H. K., Qi, B., & Yuan, Z. (2016). Practical challenges in quantum key distribution. npj Quantum Information, 2(1), 1-12.

[4] Slussarenko, S., & Pryde, G. J. (2019). Photonic quantum information processing: A concise review. Applied physics reviews, 6(4).

[5] Meher, N., & Sivakumar, S. (2022). A review on quantum information processing in cavities. The European Physical Journal Plus, 137(8), 985.

[6] Joshi, A., Noh, K., & Gao, Y. Y. (2021). Quantum information processing with bosonic qubits in circuit QED. Quantum Science and Technology, 6(3), 033001.

[7] Arakawa, Y., & Holmes, M. J. (2020). Progress in quantum-dot single photon sources for quantum information technologies: A broad spectrum overview. Applied Physics Reviews, 7(2).

[8] Kurz, C., Schug, M., Eich, P., Huwer, J., Müller, P., & Eschner, J. (2014). Experimental protocol for high-fidelity heralded photon-to-atom quantum state transfer. Nature communications, 5(1), 5527.

[9] Deng, F. G., Ren, B. C., & Li, X. H. (2017). Quantum hyperentanglement and its applications in quantum information processing. Science bulletin, 62(1), 46-68.

[10] Deng, D. L., Li, X., & Das Sarma, S. (2017). Quantum entanglement in neural network states. Physical Review X, 7(2), 021021.

[11] Erhard, M., Krenn, M., & Zeilinger, A. (2020). Advances in high-dimensional quantum entanglement. Nature Reviews Physics, 2(7), 365-381.

[12] Axline, C. J., Burkhart, L. D., Pfaff, W., Zhang, M., Chou, K., Campagne-Ibarcq, P., ... & Schoelkopf, R. J. (2018). On-demand quantum state transfer and entanglement between remote microwave cavity memories. Nature Physics, 14(7), 705-710.

[13] Li, B., Cao, Y., Li, Y. H., Cai, W. Q., Liu, W. Y., Ren, J. G., ... & Pan, J. W. (2022). Quantum state transfer over 1200 km assisted by prior distributed entanglement. Physical review letters, 128(17), 170501.

[14] Sebens, C. T. (2019). Electromagnetism as quantum physics. Foundations of Physics, 49, 365-389.

[15] Bhattacharjee, P. K. (2023). Fundamental to electromagnetic waves. International Journal of Trend in Scientific Research and Development, 7, 454-462.

[16] Casariego, M., Cruzeiro, E. Z., Gherardini, S., Gonzalez-Raya, T., André, R., Frazão, G., ... & Omar, Y. (2023). Propagating quantum microwaves: towards applications in communication and sensing. Quantum Science and Technology, 8(2), 023001.

[17] Cui, W. (2022, December). Modern Electromagnetic Field Theory and Its Application in Future Wireless Communication. In Journal of Physics: Conference Series (Vol. 2386, No. 1, p. 012044). IOP Publishing.

[18] Pirandola, S., & Braunstein, S. L. (2016). Physics: Unite to build a quantum Internet. Nature, 532(7598), 169-171.

[19] Rueda, A., Hease, W., Barzanjeh, S., & Fink, J. M. (2019). Electro-optic entanglement source for microwave to telecom quantum state transfer. npj Quantum Information, 5(1), 108.

[20] Slepyan, G., Boag, A., Mordachev, V., Sinkevich, E., Maksimenko, S., Kuzhir, P., ... & Maffucci, A. (2017). Anomalous electromagnetic coupling via entanglement at the nanoscale. New Journal of Physics, 19(2), 023014.

[21] H. Eslami & M. Mohamadian. (2024). Optimization of the positron emission tomography image resolution by using quantum entanglement concept. The European Physical Journal Plus,139(11),976-976.

[22] Antonia Tsili,Georgios Maragkopoulos,Aikaterini Mandilara & Dimitris Syvridis. (2025). Learning the N-Input Parity Function with a Single-Qubit and Single-Measurement Sampling. Electronics,14(5),901-901.

[23] Hui Cao,Dong Zhao,Ming Fang,Huang Guo,Yonghong Hu,Fangmei Liu... & Houhua Xiong. (2019). Unidirectional Invisibility Induced by Complex Anti-Parity–Time Symmetric Periodic Lattices. Applied Sciences,9(18),

[24] Xu Deng,Kai Kai Zhang,Tong Zhang,Tao Shui & Wen Xing Yang. (2025). Nonreciprocal unconventional photon blockade via Barnett effect in a hybrid cavity magnonic system. Chaos, Solitons and Fractals: the interdisciplinary journal of Nonlinear Science, and Nonequilibrium and Complex Phenomena,191,115880-115880.